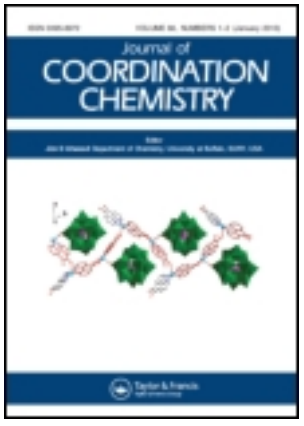

Journal of Coordination Chemistry
Publication details, including instructions for authors and subscription information:
http://www.tandfonline.com/loi/gcoo20

Hydrothermal syntheses and crystal structures of crystalline catalysts based on 3-D Ln^{3+}-pdc^{2-} frameworks and $[BW_{12}O_{40}]^{5-}$ and their heterogeneous photocatalytic oxidation of thiophene

Wei-Ning Li [a], Feng Lin [b], Xing-Xing Li [a], Lan-Cui Zhang [a], Wan-Sheng You [a] & Zong-Xuan Jiang [b]

[a] Institute of Chemistry for Functionalized Materials, Liaoning Normal University, Dalian, P.R. China

[b] Dalian Institute of Chemical Physics, The Chinese Academy of Sciences, Dalian, P.R. China

Accepted author version posted online: 19 Jun 2013.Published online: 17 Jul 2013.

To cite this article: Wei-Ning Li, Feng Lin, Xing-Xing Li, Lan-Cui Zhang, Wan-Sheng You & Zong-Xuan Jiang (2013) Hydrothermal syntheses and crystal structures of crystalline catalysts based on 3-D Ln^{3+}-pdc^{2-} frameworks and $[BW_{12}O_{40}]^{5-}$ and their heterogeneous photocatalytic oxidation of thiophene, Journal of Coordination Chemistry, 66:16, 2829-2842, DOI: 10.1080/00958972.2013.816418

To link to this article: http://dx.doi.org/10.1080/00958972.2013.816418

Journal of Coordination Chemistry, 2013
Vol. 66, No. 16, 2829–2842, http://dx.doi.org/10.1080/00958972.2013.816418

Hydrothermal syntheses and crystal structures of crystalline catalysts based on 3-D Ln^{3+}–pdc^{2-} frameworks and $[BW_{12}O_{40}]^{5-}$ and their heterogeneous photocatalytic oxidation of thiophene

WEI-NING LI†, FENG LIN‡, XING-XING LI†, LAN-CUI ZHANG†, WAN-SHENG YOU*† and ZONG-XUAN JIANG*‡

†Institute of Chemistry for Functionalized Materials, Liaoning Normal University, Dalian, P.R. China

‡Dalian Institute of Chemical Physics, The Chinese Academy of Sciences, Dalian, P.R. China

(*Received 19 March 2013; in final form 10 May 2013*)

Five $[BW_{12}O_{40}]^{5-}$-containing metal-organic frameworks (MOFs), $\{K[Ln(H_2O)_4(pdc)]_4\}[BW_{12}O_{40}]\cdot 2H_2O$ (Ln=La **1** and Ce **2**, H_2pdc = pyridine-2,6-dicarboxylate) and $\{K[Ln(H_2O)_3(pdc)]_4\}[BW_{12}O_{40}]\cdot 6H_2O$ (Ln=Tb **3**, Dy **4** and Er **5**), are synthesized hydrothermally. Ln^{3+} and pdc^{2-} are built into 3-D MOF segments containing large channels and cavities which are occupied by $[BW_{12}O_{40}]^{5-}$. Herein, we report MOF-containing polyoxometalates (POMs) as photocatalysts to oxidize thiophene with O_2 as the oxidant. Photo-excited state species ($[BW_{12}O_{40}]^{5-*}$) are generated under UV irradiation and then H_2O is oxidized into $OH^{\cdot}$ radicals and O_2 is reduced into O_2^{2-}. The active oxygen species (O_2^{2-}, $OH^{\cdot}$) oxidize thiophene in the presence of photocatalysts and SO_3, CO_2, and H_2O are obtained as photoproducts. ESR measurements provide evidence that $OH^{\cdot}$ species are generated during photocatalysis.

Keywords: Polyoxometalate; Lanthanide polymer; MOF; Photocatalysis; Desulfurization

1. Introduction

Desulfurization of various petroleum fractions has been an important research subject, due to the increasingly stringent regulations and fuel specifications in many countries for environmental protection [1, 2]. Oxidative desulfurization (ODS) is one of the most promising desulfurization processes, since it requires mild conditions of temperature and pressure [3]. Polyoxometalates (POMs), nanosized metal-oxygen cluster anions with intriguing structures, and diverse properties have been attracting worldwide attention for their effectiveness [4]. In recent years, ODS catalyzed by Keggin-type POMs have been studied and it should be a potential technology in industrialization. Salts or acids of POMs have been used as homogeneous catalysts in H_2O_2-based oxidation of dibenzothiophene (DBT) and its derivatives [5, 6]. To achieve higher activities and improve the efficiency of

*Corresponding authors. Email: wsyou@lnnu.edu.cn (W.-S. You); zxjiang@dicp.ac.cn (Z.-X. Jiang)

H_2O_2 during the oxidative process, C. Li *et al.* designed amphiphilic catalysts by combining quaternary ammonium cations with the anions of POMs [7–13]. Although homogeneous catalysts are remarkably efficient in ODS processes, it is difficult to recycle the used catalysts. For the overall process economy, it is essential to develop efficient heterogeneous catalysts and immobilize homogeneous catalysts [14–26].

Many compounds in which POMs are introduced into metal-organic frameworks (MOFs) have been reported for structures [27–30]. These materials exhibit excellent dispersity at the molecular level and high immobilization of POMs; they can also enhance the catalytic properties of heterogeneous catalysts in oxidation and esterolysis reactions [31–33]. Jhung *et al.* have reported that the adsorptive ability of Cu-BTCs (BTC: 1,3,5-benzenetricarboxlic acid) to benzothiophene is improved when loading with $[PW_{12}O_{40}]^{3-}$, which results from favorable acid–base effect between $[PW_{12}O_{40}]^{3-}$ and slightly basic benzothiophene [34]. POM-containing MOF catalysts have not been reported in the ODS processes. We have achieved five $[BW_{12}O_{40}]^{5-}$-containing MOF compounds which are synthesized hydrothermally and characterized by IR, UV–visible diffuse reflectance spectra (UV–vis DRS), TG analysis, and powder X-ray diffraction (PXRD). Photocatalytic oxidation for thiophene has also been investigated under UV irradiation using O_2 as oxidant.

2. Experimental

2.1. *Materials and general methods*

$K_5BW_{12}O_{40}\cdot 14H_2O$ was synthesized according to the literature method and identified by IR spectrum [35]. All other chemicals were purchased commercially and used without purification. Elemental analyses were determined by a Perkin–Elmer 2400 CHN elemental analyzer. IR spectra were recorded from 400 to 4000 cm^{-1} on a TENSOR27 Bruker AXS spectrometer with pressed KBr pellets. TG-DTA analyses were carried out on a Pyris Diamond TG/DTA instrument in air from 25 to 900 °C with a heating rate of 10 °C min^{-1}. PXRD patterns were recorded on a Japan Rigaku D/max γA X-ray diffractometer equipped with graphite monochromated Cu Kα radiation ($\lambda = 1.5406$ Å). UV–visible diffuse reflectance spectra (UV–vis DRS) were obtained on a UV–vis spectrophotometer (JASCO V-550) with an integrating sphere from 190 to 900 nm. ESR signals of radicals trapped by DMPO (5,5-dimethyl-l-pyrroline-*N*-oxide) were performed on a Bruker ESR A200 spectrometer at ambient temperature. After bubbling O_2 for 10 min, the samples were introduced into the homemade quartz cup inside the microwave cavity and illuminated with a 300 W Xe lamp (CERAMAX LX-300).

2.2. *Synthesis of {K[La(H$_2$O)$_4$(pdc)]$_4$}[BW$_{12}$O$_{40}$]·2H$_2$O (1)*

A mixture of $La(NO_3)_3\cdot 6H_2O$ (0.4 mM, 0.17 g), $K_5BW_{12}O_{40}\cdot 14H_2O$ (0.15 mM, 0.5 g), H_2pdc (0.35 mM, 0.05 g) and water (10 mL) was sealed in a 15 mL Teflon reactor under autogenous pressure at 120 °C for 4 days. After cooling the mixture to room temperature, colorless crystals were obtained in 45.2% yield (0.81 g, based on W). Anal. Calcd for $KC_{28}H_{48}La_4N_4O_{74}BW_{12}$ (%): C, 7.57; H, 1.08; N, 1.26. Found (%): C, 7.55; H, 1.09; N, 1.25.

2.3. *Synthesis of $\{K[Ce(H_2O)_4(pdc)]_4\}[BW_{12}O_{40}]\cdot 2H_2O$ (2)*

The synthetic procedure of **2** was similar to that of **1** except that $Ce(NO_3)_3\cdot 6H_2O$ (0.4 mM, 0.17 g) replaced $La(NO_3)_3\cdot 6H_2O$. Yellow crystals were obtained in 47.8% yield (0.85 g, based on W). Anal. Calcd for $KC_{28}H_{48}Ce_4N_4O_{74}BW_{12}$ (%): C, 7.56; H, 1.08; N, 1.26. Found (%): C, 7.55; H, 1.10; N, 1.24.

2.4. *Synthesis of $\{K[Tb(H_2O)_3(pdc)]_4\}[BW_{12}O_{40}]\cdot 6H_2O$ (3)*

The synthetic procedure of **3** was similar to that of **1** except that $Tb(NO_3)_3\cdot 5H_2O$ (0.4 mM, 0.17 g) replaced $La(NO_3)_3\cdot 6H_2O$. Colorless crystals were obtained in 45.3% yield (0.82 g, based on W). Anal. Calcd for $KC_{28}H_{48}Tb_4N_4O_{74}BW_{12}$ (%): C, 7.44; H, 1.06; N, 1.24. Found (%): C, 7.42; H, 1.08; N, 1.23.

2.5. *Synthesis of $\{K[Dy(H_2O)_3(pdc)]_4\}[BW_{12}O_{40}]\cdot 6H_2O$ (4)*

The synthetic procedure of **4** was similar to that of **1** except that $Dy(NO_3)_3\cdot 6H_2O$ (0.4 mM, 0.18 g) replaced $La(NO_3)_3\cdot 6H_2O$. Colorless crystals were obtained in 43.7% yield (0.79 g, based on W). Anal. Calcd for $KC_{28}H_{48}Dy_4N_4O_{74}BW_{12}$ (%): C, 7.42; H, 1.06; N, 1.24. Found (%): C, 7.41; H, 1.08; N, 1.23.

2.6. *Synthesis of $\{K[Er(H_2O)_3(pdc)]_4\}[BW_{12}O_{40}]\cdot 6H_2O$ (5)*

The synthetic procedure of **5** was similar to that of **1** except that $Er(NO_3)_3\cdot 6H_2O$ (0.4 mM, 0.18 g) replaced $La(NO_3)_3\cdot 6H_2O$. Pink crystals were obtained in 42.8% yield (0.78 g, based on W). Anal. Calcd for $KC_{28}H_{48}Er_4N_4O_{74}BW_{12}$ (%): C, 7.38; H, 1.05; N, 1.23. Found (%): C, 7.36; H, 1.06; N, 1.22.

2.7. *X-ray crystallographic study*

Crystal data of **1**–**5** were collected with a SMART APEX II-CCD X-ray single crystal diffractometer at 293 K with graphite-monochromatic Mo Kα radiation ($\lambda = 0.71073$ Å). The structures were solved by direct methods and refined by full-matrix least squares on F^2 using SHELXS-97. Non-hydrogen atoms were refined anisotropically and hydrogens attached to carbon were added theoretically. A summary of the crystallographic data is shown in table 1.

2.8. *Photocatalytic reaction*

Photocatalytic oxidations of thiophene were performed in a homemade Pyrex reaction cell with O_2 bubbled in a constant flow as oxidant. To 150 mL of acetonitrile solution containing thiophene ($[\text{sulfur content}]_{\text{initial}} = 200$, 400, and 600 ppm), the photocatalyst (150 mg) was added. The suspension was stirred in the dark for 30 min to establish adsorption/desorption equilibrium between the solution and photocatalyst, then irradiated by a 125 W high pressure mercury lamp. The temperature of the mixture was 5 ± 2 °C maintained by a flow of cooling water. After removing the photocatalyst by centrifugation, photoproducts were identified by GC-FPD (Agilent 7890, FFAP column).

Table 1. Crystallographic data for **1**–**5**.

	1	**2**	**3**	**4**	**5**
Formula	$KC_{28}H_{48}La_4N_4O_{74}BW_{12}$	$KC_{28}H_{48}Ce_4N_4O_{74}BW_{12}$	$KC_{28}H_{48}Tb_4N_4O_{74}BW_{12}$	$KC_{28}H_{48}Dy_4N_4O_{74}BW_{12}$	$KC_{28}H_{48}Er_4N_4O_{74}BW_{12}$
Formula weight	4436.33	4441.29	4516.49	4530.81	4549.85
Crystal system	Monoclinic	Monoclinic	Tetragonal	Tetragonal	Tetragonal
Space group	*C2/c*	*C2/c*	*I* $4_1/a$	*I* $4_1/a$	*I* $4_1/a$
a (Å)	30.778(7)	30.685(2)	21.8788(13)	21.8108(8)	21.781(2)
b (Å)	15.587(3)	15.5835(10)	21.8788(13)	21.8108(8)	21.781(2)
c (Å)	22.103(5)	22.0529(14)	16.1443(19)	16.0953(12)	16.101(3)
α (°)	90	90	90	90	90
β (°)	132.995(5)	132.9840(10)	90	90	90
γ (°)	90	90	90	90	90
V (Å^3)	7756(3)	7714.3 (9)	7728.0 (11)	7656.7 (7)	7638.7(19)
Z	4	4	4	4	4
D_c (Mg m^{-3})	3.799	3.824	3.882	3.930	3.956
μ (mm^{-1})	20.047	20.300	21.568	21.978	22.511
F (0 0 0)	7901	7920	8032	8048	8080
Reflns. collected	19,080	26,766	19,110	23,428	18,835
Unique reflns.	6824	6775	3416	4715	3356
R_{int}	0.0873	0.0407	0.0758	0.0698	0.0663
GOF on F^2	1.048	1.145	1.012	1.057	1.062
R_1 [$I>2\sigma$ (I)]	0.0997	0.0856	0.0404	0.0299	0.0306
wR_2 [$I>2\sigma$ (I)]	0.2143	0.2057	0.0983	0.0609	0.0719
R_1 (all data)[a]	0.1430	0.1172	0.0497	0.0463	0.0387
wR_2 (all data)[b]	0.2313	0.2190	0.1023	0.0654	0.0747

[a] $R-1=\sum||F_0|-|F_c||/\sum|F_0|$; [b] $wR_2=[\sum\omega(F_0-F_c)^2/\sum\omega(F_0^2)^2]^{1/2}$.

3. Results and discussion

3.1. *Crystal structure description*

Single crystal X-ray diffraction analysis reveals that **1**–**5** consist of discrete $[BW_{12}O_{40}]^{5-}$ anions, 3-D Ln^{3+}–pdc^{2-}–H_2O cationic frameworks and K^+. $[BW_{12}O_{40}]^{5-}$ exhibit the well-known α-Keggin structure [36, 37] which is formed from twelve WO_6 octahedra and one BO_4 tetrahedron. For **1** and **2**, the central B is located at the inversion center, surrounded by a cube of eight oxygens with each oxygen site half-occupied. For **3**–**5**, it is surrounded by a tetrahedron of four oxygens with each oxygen site fully occupied. All B–O and W–O bond lengths are in normal ranges (tables S1–S5).

1 and **2** are isostructural and crystallize in the monoclinic system and *C2/c* space group. They are isomorphic with $[Ln(H_2O)_4(pdc)]_4[XMo_{12}O_{40}]$ (**6**) (Ln=La, Ce, and Nd; X=Si and Ge) [38] and $[Ln(H_2O)_3Ln(H_2O)_4(pdc)_2]_2[SiW_{12}O_{40}]$ (**7**) (Ln=Eu, Gd, Tb, Dy) [39]. **1** has been selected as the example to describe crystal structures of **1** and **2**. As shown in figure 1, the 3-D $[La(H_2O)_4(pdc)]^+$ cationic framework in **1** is identical with that of **6**. There are two crystallographically independent La^{3+} centers (La1 and La2) with similar coordination environments. The nine-coordinate La^{3+} coordinates to one nitrogen of pdc^{2-}, four oxygens of carboxyl groups of three different pdc^{2-}, and four waters. Each pdc^{2-} adopts an exo-tridentate coordination. The La–O and La–N distances are similar to those found in **6**. As shown in figure 2, the 3-D $[La(H_2O)_4(pdc)]^+$ cationic framework shows the zeolite-like GIS topological structure [38]. Viewed along the *c* axis, $[BW_{12}O_{40}]^{5-}$ anions are arrayed in nonuniform channels of the zeolite-like structure in a zigzag fashion. Since $[BW_{12}O_{40}]^{5-}$ has one more negative charge than $[XMo_{12}O_{40}]^{4-}$ in **6**, K^+ ions are necessary to balance the charge in **1**. As shown in figure 3, K^+ ions are located in $[La(H_2O)_4(pdc)]^+$ frameworks in a six-coordinate octahedral configuration. The four equatorial

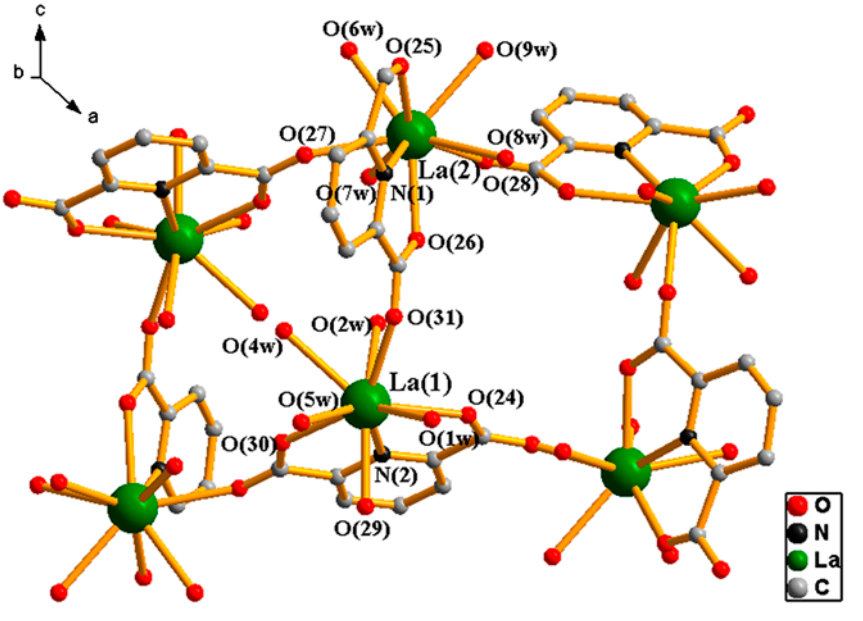

Figure 1. Coordination mode of two crystallographically independent La^{3+} centers in **1**. Hydrogens are omitted for clarity.

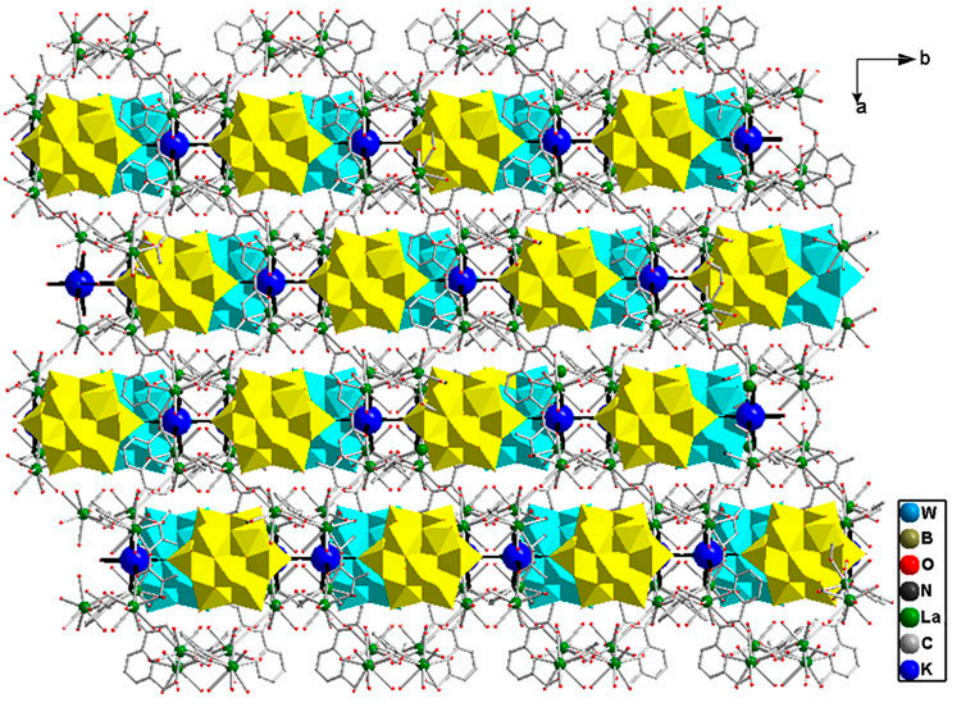

Figure 2. Channels of the zeolite-like structure in a zigzag fashion occupied by $[BW_{12}O_{40}]^{5-}$ along the *c* axis in **1**. Polyhedra: $[BW_{12}O_{40}]^{5-}$.

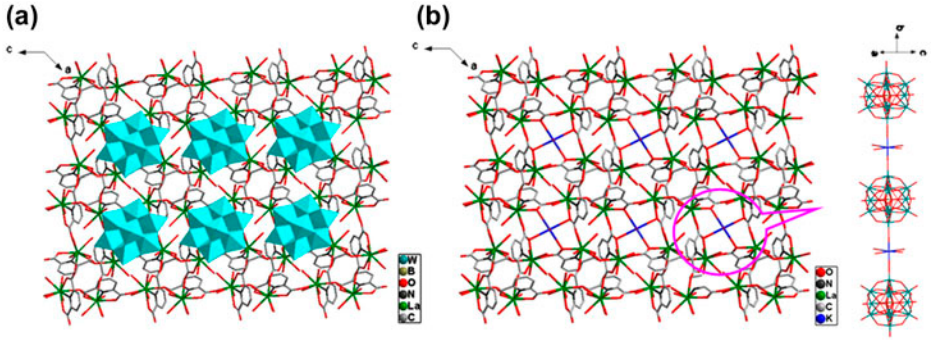

Figure 3. View of the 3-D framework of **1** along the *b* axis. (a) $[BW_{12}O_{40}]^{5-}$ occupy cavities and (b) octahedral coordination environment of K^+ in cavities. Polyhedra: $[BW_{12}O_{40}]^{5-}$.

positions are occupied by four oxygens of carboxyl groups and K–O distances are 2.90 (2)–2.99(2) Å. The two axial positions are occupied by two terminal oxygens of $[BW_{12}O_{40}]^{5-}$ and K–O distances are 2.57(5)–2.75 (3) Å. $[BW_{12}O_{40}]^{5-}$ are linked into 1-D chains along the *b* axis through K^+ ions (see inset in figure 3).

Solids **3**, **4**, and **5** are isostructural and crystallize in tetragonal system and *I* $4_1/a$ space group. They are isomorphic with $[Ln(H_2O)_4(pdc)]_4[SiW_{12}O_{40}]$ (**8**) (Ln=La, Ce, Nd) [40]. **4** has been selected as the example to describe crystal structures of **3**, **4,** and **5**. As shown in

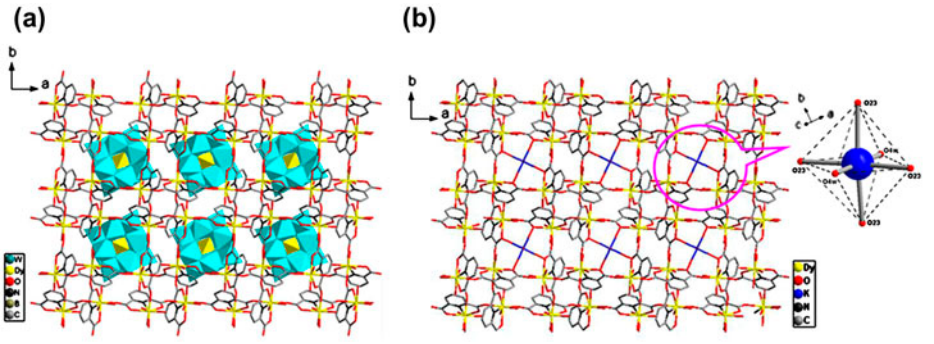

Figure 4. Packing of the 3-D framework of **4** long the *c* axis. (a) The cavities of intersected channels occupied by $[BW_{12}O_{40}]^{5-}$ and (b) octahedral coordination environment of K^+ in cavities. Polyhedra: $[BW_{12}O_{40}]^{5-}$.

figure 4, Dy^{3+} and pdc^{2-} are built into a 3-D $[Dy(H_2O)_3(pdc)]^+$ architecture in **4**, similar to that of **8**. Eight-member channels are found along the *c* axis in the 3-D cationic network. They intersect to form large cavities, which array in a zigzag fashion and are occupied by nanosized $[BW_{12}O_{40}]^{5-}$. Due to lanthanide contraction, Tb^{3+}, Dy^{3+}, and Er^{3+} exhibit a lower coordination number than those of **8** and all have eight-coordinate environments in **3**, **4**, and **5**, with one nitrogen of a pdc^{2-}, four oxygens of carboxyl of three different pdc^{2-} ligands, and three waters. K^+ ions are necessary to balance the charge in **4** and also are six-coordinate. The four equatorial positions are occupied by four oxygens of carboxyl and two axial positions are occupied by water; K–O (pdc) distances are 2.997(8)–3.022(10) Å and K–O (water) distances are 2.479(16)–2.500(19) Å.

3.2. *IR spectra*

IR spectra are shown in figure S1 and similar IR peaks have been observed for **1**–**5**. The characteristic peaks at ~961, ~908, ~825, and ~761 cm^{-1} are attributed to ν(W–Od), ν(B–Oa), ν(W–Ob) and ν(W–Oc), respectively [41]; 1616–1286 cm^{-1} can be regarded as carboxylic groups of pdc^{2-}.

3.3. *TG analysis*

To investigate the thermal stabilities of **1**–**5**, TG/DTA measurements are performed (figure S2). From 30 to 109 °C, **1** loses two crystallization waters, the weight loss of 0.85% agrees with the calculated value of 0.81%. The weight loss of 5.24% between 109 and 150 °C is attributed to loss of thirteen coordinated waters (calcd 5.27%). The weight loss of 4.93% corresponds to the loss of another coordinated water and one pdc^{2-} from 150 to 575 °C (calcd 4.94%). Then, decomposition of the framework occurs at 575 °C. **2** shows similar weight loss steps as **1** and the total weight loss is 11.08% (Calcd 11.01%). **3** shows a 4.37% weight loss between 30 and 106 °C which corresponds to six crystallographic waters and five coordinated waters (Calcd 4.38%). The weight loss of 6.47%, when temperature changes from 106 to 597 °C ascribes to the release of the other coordinated water and one pdc^{2-}. **4** and **5** exhibit similar weight loss stages as **3** with mass losses of 10.88% (Calcd 10.79%) and 10.76% (Calcd 10.75%), respectively.

3.4. *PXRD analysis*

Experimental and simulated PXRD patterns of **1**-**5** are shown in figure S3. The diffraction peaks match well in key positions, which indicate the crystal phase purity. For some peaks, difference in intensity may be caused by preferred orientation of the powder samples.

3.5. *UV–vis DRS*

UV–visible diffuse reflectance spectra of **1**–**5** are shown in figure S4. **1**–**5** absorb UV light with wavelength shorter than ~400 nm. By using this value, the band gap is calculated as $E_g = 3.11$ eV. Photonic activation can carry out when light energy is higher than 3.11 eV.

3.6. *Photocatalytic oxidation of thiophene*

As one of the main sulfur-containing compounds in gasoline, thiophene is difficult to be oxidized by traditional ODS methods. The inertness of thiophene in oxidation is mainly due to its aromaticity and the low electron density of sulfur [42]. Here, thiophene was selected as the test model. The photocatalytic oxidation of thiophene ($[\text{sulfur content}]_{\text{initial}} = 200$ ppm) was performed in acetonitrile under UV irradiation and O_2 was bubbled into the system in a constant flow. As shown in figure 5, a blank experiment was carried out without the photocatalyst and the conversion of thiophene was 25% for 12 h. However, when **1**–**5** ($1\ \text{g L}^{-1}$) were added to the reaction, the conversions of thiophene reached to ca. 49, 97, 68, 46, and 42%, respectively, with **2** exhibiting the highest catalytic activity. It may result from synergistic effect between Ce^{3+}–pdc^{2+} framework and $[BW_{12}O_{40}]^{5-}$ anions.

2 was selected as the photocatalyst for further experiments. For identification of the photoproducts, the gas from the reaction mixture was injected into NaOH solution (0.2 M). After the reaction, $Ba(NO_3)_2$ aqueous solution (0.2 M) was added into the NaOH solution

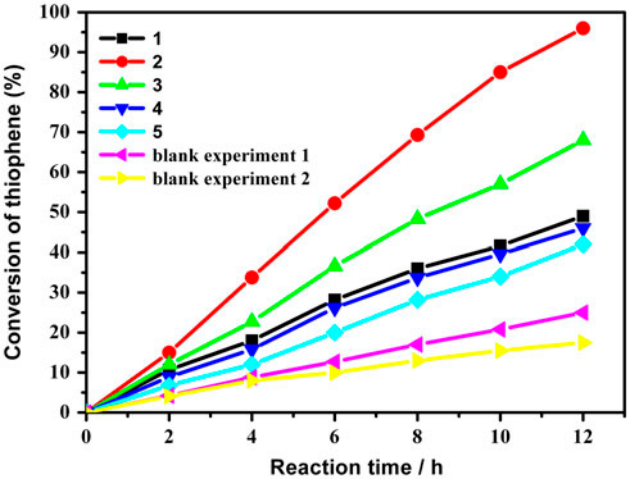

Figure 5. Photocatalytic oxidation of thiophene on different photocatalysts under UV irradiation. Reaction conditions: the concentration of photocatalyst: $1\ \text{g L}^{-1}$; $[\text{sulfur content}]_{\text{initial}} = 200$ ppm; O_2 (bubbled into the system); reaction time: 12 h. Blank experiment 1 was carried out under the same conditions, except without the photocatalyst. Blank experiment 2 was carried out under the same conditions except without light.

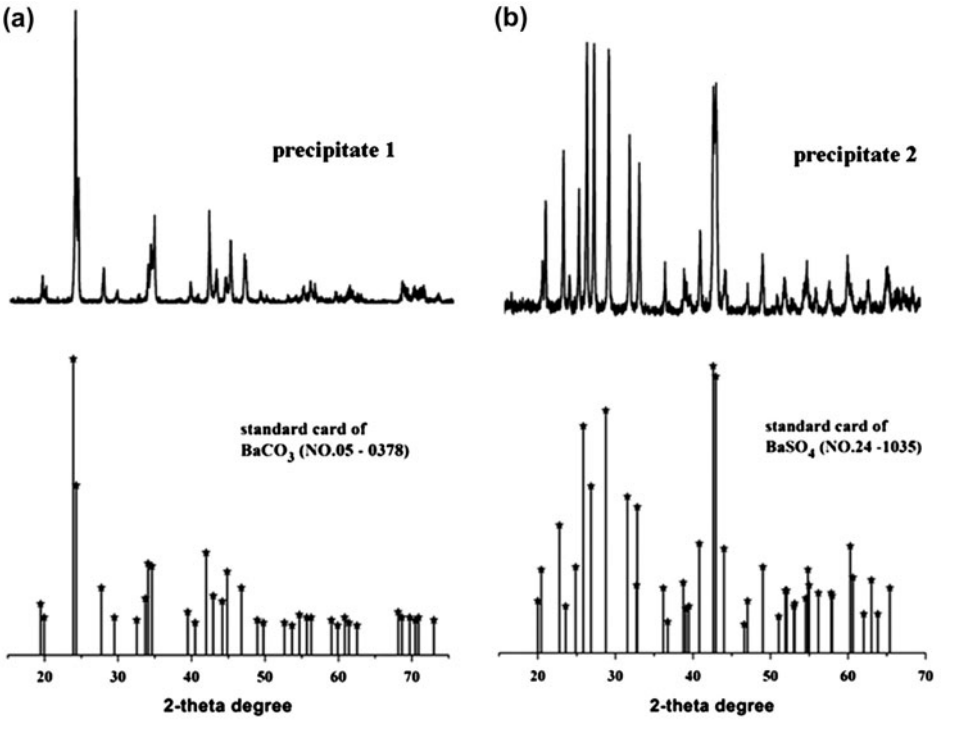

Figure 6. XRD patterns of the produced precipitates (top) and the standard cards (bottom). The gas produced in the reaction system was absorbed by NaOH aqueous solution (0.2 M), then $Ba(NO_3)_2$ (aq) (0.2 M) and HNO_3 (aq) were added successively to produce the precipitates 1 and 2. Reaction conditions: the concentration of **2**: 1 g L^{-1}; $[\text{sulfur content}]_{\text{initial}} = 200$ ppm; O_2 (bubbled into the system).

and a white precipitate (denoted as precipitate 1) was obtained. The XRD pattern was assigned to $BaCO_3$ (figure 6(a)) which is referred to the standard card (PDF#05-0378) taken from the Joint Committee on Powder Diffraction Standards (JCPDS) Database. The result suggested CO_2 was a photocatalytically oxidized product of thiophene and escaped from the reaction system. However, when precipitate 1 was treated with HNO_3 (aq), there was still some white precipitate (denoted as precipitate 2) in the solvent. The XRD pattern of precipitate 2 was assigned to $BaSO_4$ (figure 6(b)) and the peaks matched well with the standard JCPDS database (PDF#24-1035). The result indicated that SO_3 was the other photoproduct in this reaction. Based on the above results, thiophene can be oxidized to CO_2 and SO_3 in the photocatalytic oxidation.

To investigate the heterogeneous catalytic characteristics, **2** was immersed in acetonitrile solution containing thiophene ($[\text{sulfur content}]_{\text{initial}} = 200$ ppm) for 6 h. Then **2** was filtered off and the filtrate was used for the photocatalytic reaction under UV irradiation. As shown in figure 7, the conversion of thiophene was similar to that of the blank experiment. This result revealed that **2** could not dissolve in the reaction solution and was a heterogeneous catalyst in photocatalytic oxidation of thiophene. Recycling experiments of **2** were also carried out. After the first run for 10 h was completed, the photocatalyst was separated from the reaction system by centrifugation and then added to fresh acetonitrile solution containing 200 ppm of thiophene forming a new reaction system for the next run. The

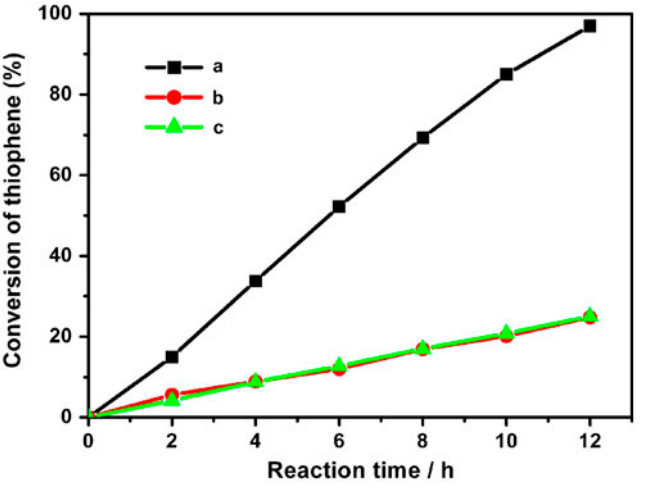

Figure 7. (a) Photocatalytic oxidation of thiophene for **2**. Reaction conditions: the concentration of photocatalyst: 1 g L^{-1}; [sulfur content]$_{initial}$ = 200 ppm; O_2 (bubbled into the system); reaction time: 12 h. (b) The experiment was performed under the same conditions except that the photocatalyst was filtered after immersing in the experiment solution for 6 h. (c) Blank experiment was carried out under the same conditions except without photocatalyst.

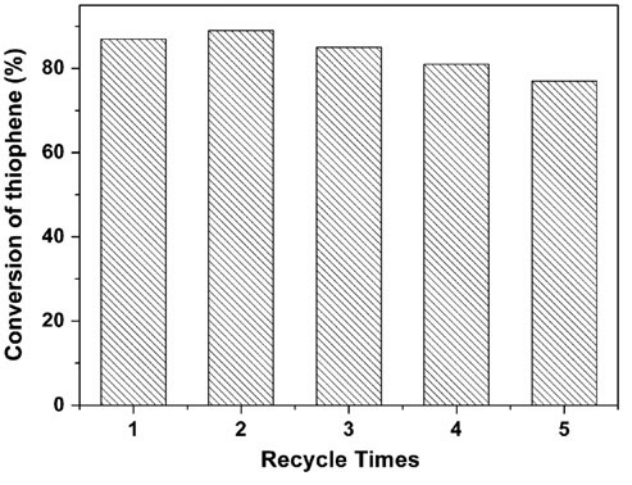

Figure 8. The recycle times on the conversion of thiophene with **2** as photocatalyst. Reaction conditions: [sulfur content]$_{initial}$ = 200 ppm; the concentration of photocatalyst: 1 g L^{-1}; O_2 (bubbled into the system); reaction time: 10 h.

photocatalytic activity decreased slightly with the conversion of 87.3, 89.1, 84.5, 80.6, and 77.2% for 10 h, respectively. Thus. the photocatalyst could be recycled (figure 8).

For application of ultra-low-sulfur-containing fuels, it is essential to investigate the influence of initial sulfur content on the conversion for photocatalytic oxidation of thiophene. As shown in figure 9, reactions with different initial sulfur contents ([sulfur content]$_{initial}$ = 200, 400, and 600 ppm) were performed. When the initial sulfur content was

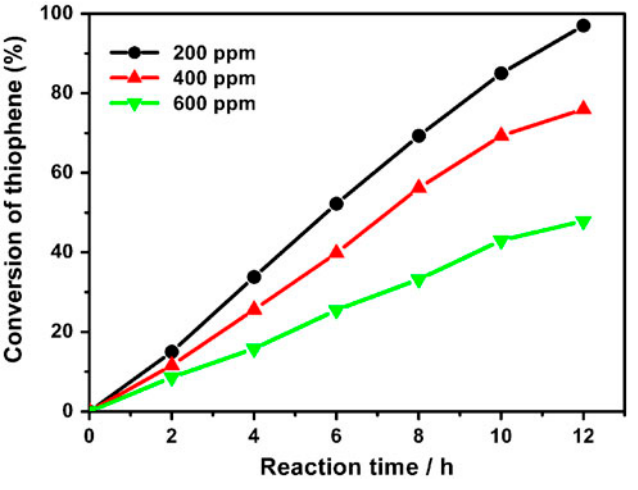

Figure 9. Photocatalytic oxidation activity of thiophene for **2** with different initial sulfur content ([sulfur content]$_{initial}$ = 200, 400, and 600 ppm). Reaction conditions: the concentration of photocatalyst: 1 g L^{-1}; O_2 (bubbled into the system); reaction time: 12 h.

200 ppm, thiophene was oxidized 97% for 12 h under UV irradiation. The conversions of thiophene reached to 76 and 47.9%, respectively, when the initial sulfur contents increased to 400 and 600 ppm for 12 h.

Comparing the activity of **2** with that of commercial P25 for photocatalytic oxidation of thiophene, conversion of thiophene reaches to 43% in 5 h under 125 W high pressure mercury lamp illumination for **2** and 48% in 5 h under 500 W high pressure mercury lamp illumination for P25 [43]. In addition, specific surface area of **2** is lower than that of P25. Therefore, MOF's POMs may be comparable photocatalysts for photocatalytic ODS.

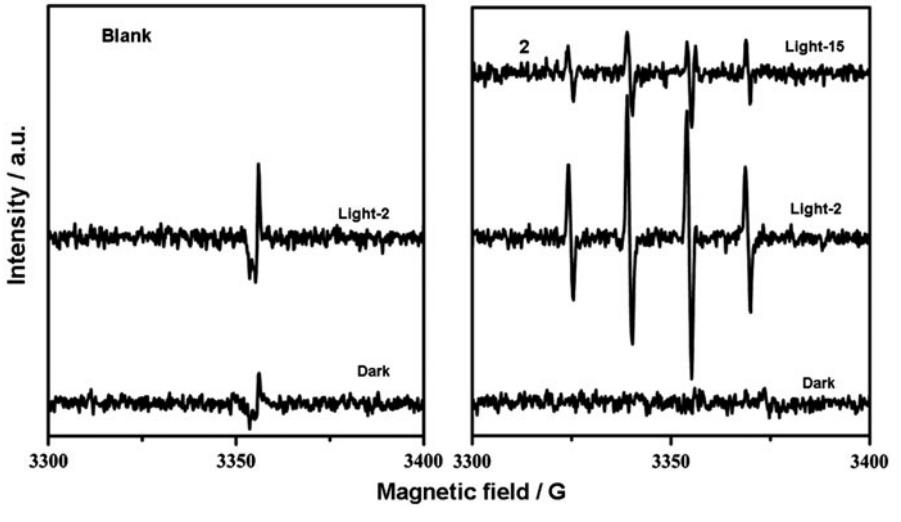

Figure 10. ESR spectra of the DMPO–OH adduct generated in the photocatalytic oxidation reaction of thiophene. The sample tested without photocatalyst is denoted as "Blank". The signals obtained without UV irradiation are denoted as "Dark". The signals obtained under irradiation for 2 min are denoted as "Light-2" and that for 15 min named "Light-15".

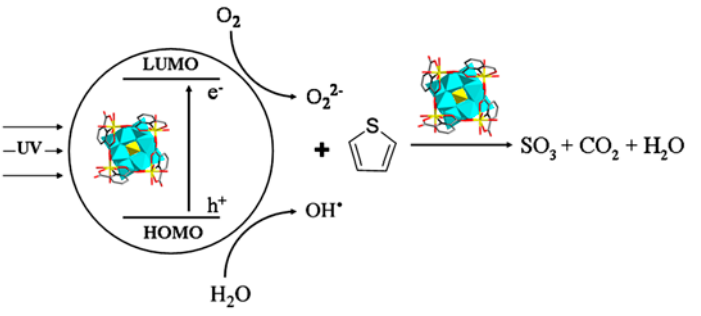

Figure 11. Brief description of the mechanism for photocatalytic oxidation of thiophene on Ln^{3+}–pdc^{2-} $[BW_{12}O_{40}]^{5-}$. Polyhedra indicate the crystalline catalyst used in the reaction.

3.7. *Proposed reaction mechanism for photocatalytic oxidation of thiophene*

ESR spin-trap with DMPO is a useful technique to monitor active oxygen species generated in the reaction system. ESR signals obtained from the *in-situ* photocatalytic reaction of **2** are shown in figure 10. No ESR signals were observed either when there was no photocatalyst or the reaction was performed with **2** in the dark. After 2 min of illumination, ESR signals were centered at $g = 2.0065$ in the presence of **2**, which can be assigned to active oxygen species [44]. The typical quartets with intensity of 1 : 2 : 2 : 1 indicated that the DMPO–OH adduct was formed during the reaction with hyperfine coupling constants of $\alpha^N = 14.9$ G and $\alpha^H\beta = 14.9$ G [45–47]. The intensity of the peaks decreased after illumination for 15 min, due to oxidation of the DMPO–OH adduct by holes generated during the illumination and consumption of dissolved O_2. No ESR signals of O_2^- are observed in the photocatalytic system of **2**, but both $OH^\cdot$ and O_2^- radicals are generated in the photocatalytic system of $Pt/RuO_2/TiO_2$ [48].

Figure 11 shows a brief description of the mechanism for photocatalytic oxidation of thiophene on Ln^{3+}–pdc^{2-} $[BW_{12}O_{40}]^{5-}$. The reaction is carried out under UV irradiation leading to the charge transfer (O(2p) → W(5d)) and the formation of the photo-excited state species ($[BW_{12}O_{40}]^{5-*}$) [49]. $OH^\cdot$, a non-selective and strong oxidant for photocatalytic oxidation, is generated *via* the reaction between H_2O and the photo-generated hole. The adsorbed oxygen molecules trap excited electrons forming O_2^{2-} which is ESR-silent in the reaction [48, 50]. Consequently, thiophene molecules react with the active oxygen species ($(O_2^{2-}$, $OH^\cdot)$ in the presence of **2** initiating a series of oxidation reactions. SO_3, CO_2, and H_2O are obtained as the photoproducts.

4. Conclusions

We have hydrothermally synthesized five 3-D lanthanide-linked compounds based on $[BW_{12}O_{40}]^{5-}$ and investigated their properties in heterogeneous photocatalytic oxidation of thiophene. This is the first report of MOF compounds containing POMs as photocatalysts to oxidize thiophene to SO_3 in the presence of O_2 as the oxidant. These materials present favorable catalytic properties and the oxidation of thiophene on **2** is ca. 97% in 12 h. In the mechanism for photocatalytic oxidation of thiophene, active oxygen species ($(O_2^{2-}$, $OH^\cdot)$ are crucial leading to oxidation. Such a photocatalytic oxidative application of MOF compounds containing POMs would provide a promising perspective in the advanced oxidation area.

Supplementary material

Crystallographic data for **1**–**5** have been deposited with the Cambridge Crystallographic Data Center, CCDC numbers 913822, 913823, 913824, 913825, and 913826, respectively. These data are available free of charge from The Cambridge Crystallographic Data Center *via* the Internet at www.ccdc.cam.ac.uk/data_request/cif.

Acknowledgments

This work is financially supported by the National Science Foundation of China (No. 20773057) and the National Key Basic Research and Development Program (No. 2009CB220010).

References

[1] A. Ishihara, D. Wang, F. Dumeignil, H. Amano, E.W. Qian, T. Kabe. *Appl. Catal., A*, **279**, 279 (2005).
[2] S. Mondal, Y. Hangun-Balkir, L. Alexandrova, D. Link, B. Howard, P. Zandhuis, A. Cugini, C.P. Horwitz, T.J. Collins. *Catal. Today*, **116**, 554 (2006).
[3] R. Wang, G.F. Zhang, H.X. Zhao. *Catal. Today*, **149**, 117 (2010).
[4] S.P. Liu, L. Xu, F.Y. Li, B.B. Xu, Z.X. Sun. *J. Mater. Chem.*, **21**, 1946 (2011).
[5] M. Te, C. Fairbridge, Z. Ring. *Appl. Catal., A*, **219**, 267 (2001).
[6] W. Trakarnpruk, K. Rujiraworawut. *Fuel Process. Technol.*, **90**, 411 (2009).
[7] C. Komintarachat, W. Trakarnpruk. *Ind. Eng. Chem. Res.*, **45**, 1853 (2006).
[8] J.H. Qiu, G.H. Wang, D.L. Zeng, Y. Tang, M. Wang, Y.J. Li. *Fuel Process. Technol.*, **90**, 1538 (2009).
[9] W.S. Zhu, W.L. Huang, H.M. Li, M. Zhang, W. Jiang, G.Y. Chen, C.R. Han. *Fuel Process. Technol.*, **92**, 1842 (2011).
[10] M.A. Rezvani, A.F. Shojaie, M.H. Loghmani. *Catal. Commun.*, **25**, 36 (2012).
[11] Y.N. Zhang, H.Y. Lü, L. Wang, Y.L. Zhang, P. Liu, H.X. Han, Z.X. Jiang, C. Li. *J. Mol. Catal. A: Chem.*, **332**, 59 (2010).
[12] T. Yamaura, K. Kamata, K. Yamaguchi, N. Mizuno. *Catal. Today*, **203**, 76 (2012).
[13] H.Y. Lü, J.B. Gao, Z.X. Jiang, F. Jing, Y.X. Yang, G. Wang, C. Li. *J. Catal.*, **239**, 369 (2006).
[14] Z. Eldin, A. Abdalla, B.S. Li. *Chem. Eng. J.*, **200–202**, 113 (2012).
[15] Z. Eldin, A. Abdalla, B.S. Li, A. Tufail. *Colloids Surf., A*, **341**, 86 (2009).
[16] Z.X. Zhang, F.W. Zhang, Q.Q. Zhu, W. Zhao, B.C. Ma, Y. Ding. *J. Colloid Interface Sci.*, **360**, 189 (2011).
[17] X.M. Yan, P. Mei, J.H. Lei, Y.Z. Mi, L. Xiong, L.P. Guo. *J. Mol. Catal. A: Chem.*, **304**, 52 (2009).
[18] B.S. Li, W. Ma, J.J. Liu, C.Y. Han, S.L. Zuo, X.F. Li. *Catal. Commun.*, **13**, 101 (2011).
[19] X.A. Cui, D.D. Yao, H. Li, J.X. Yang, D.D. Hu. *J. Hazard. Mater.*, **205–206**, 17 (2012).
[20] D. Huang, Y.J. Wang, Y.C. Cui, G.S. Luo. *Microporous Mesoporous Mater.*, **116**, 378 (2008).
[21] B.S. Li, Z.X. Liu, C.Y. Han, J.J. Liu, S.L. Zuo, Z.Y. Zhou, X.M. Pang. *J. Mol. Catal. A: Chem.*, **348**, 106 (2011).
[22] M. Arias, D. Laurenti, C. Geantet, M. Vrinat, I. Hideyuki, Y. Yoshimura. *Catal. Today*, **130**, 190 (2008).
[23] S.F. Song, S.K. Shen, X.A. Cui, D.D. Yao, D.D. Hu. *React. Funct. Polym.*, **71**, 51 (2011).
[24] R. Wang, F.L. Yu, G.F. Zhang, H.X. Zhao. *Catal. Today*, **150**, 37 (2010).
[25] L.N. Yang, J. Li, X.D. Yuan, J. Shen, Y.T. Qi. *J. Mol. Catal. A: Chem.*, **262**, 114 (2007).
[26] X.M. Yan, G.S. Su, L. Xiong. *J. Fuel Chem. Technol.*, **37**, 318 (2009).
[27] B.S. Li, Z.X. Liu, J.J. Liu, Z.Y. Zhou, X.H. Gao, X.M. Pang, H.T. Sheng. *J. Colloid Interface Sci.*, **362**, 450 (2011).
[28] L.M. Dai, W.S. You, Y.G. Li, E.B. Wang, C.Y. Huang. *Chem. Commun.*, **19**, 2721 (2009).
[29] L.M. Dai, W.S. You, E.B. Wang, S.X. Wu, Z.M. Su, Q.H. Du, Y. Zhao, Y. Fang. *Cryst. Growth Des.*, **9**, 2110 (2009).
[30] X.L. Wang, C. Qin, E.B. Wang, Z.M. Su, Y.G. Li, L. Angew. *Chem. Int. Ed.*, **45**, 7411 (2006).
[31] D.L. Long, E. Burkholder, L. Cronin. *J. Chem. Soc. Rev.*, **36**, 105 (2007).
[32] C.Y. Sun, S.X. Liu, D.D. Liang, K.Z. Shao, Y.H. Ren, Z.M. Su. *J. Am. Chem. Soc.*, **131**, 1883 (2009).
[33] N.V. Maksimchuk, M.N. Timofeeva, M.S. Melgunov, A.N. Shmakov, Y.A. Chesalov, D.N. Dybtsev, V.P. Fedin, O.A. Kholdeeva. *J. Catal.*, **257**, 315 (2008).
[34] N.A. Khan, S.H. Jhung. *Fuel Process. Technol.*, **100**, 49 (2012).
[35] C.R. Deltcheff, M. Fournier, R. Franck, R. Thouvenot. *Inorg. Chem.*, **22**, 207 (1983).

[36] J.Y. Niu, J.W. Zhao, J.P. Wang, P.T. Ma. *J. Mol. Struct.*, **699**, 85 (2004).
[37] H.Y. An, E.B. Wang, Y.G. Li, Z.M. Zhang, L. Inorg. *Chem. Commun.*, **10**, 299 (2007).
[38] C.H. Li, K.L. Huang, Y.N. Chi, X. Liu, Z.G. Han, L. Shen, C.W. Hu. *Inorg. Chem.*, **48**, 2010 (2009).
[39] X.Y. Liu, Y.Y. Jia, Y.F. Zhang, R.D. Huang. *Eur. J. Inorg. Chem.*, **25**, 4027 (2010).
[40] Y.Z. Gao, Y.Q. Xu, Z.G. Han, C.H. Li, F.Y. Cui, Y.N. Chi, C.W. Hu. *J. Solid State Chem.*, **183**, 1000 (2010).
[41] J.W. Zhao, Y.P. Song, P.T. Ma, J.P. Wang, J.Y. Niu. *J. Solid State Chem.*, **182**, 1798 (2009).
[42] B.Y. Zhang, Z.X. Jiang, J. Li, Y.N. Zhang, F. Lin, Y. Liu, C. Li. *J. Catal.*, **287**, 5 (2012).
[43] X.J. Wang, F.T. Li, J.X. Liu, C.G. Kou, Y. Zhao, Y.J. Hao, D.S. Zhao. *Energy Fuel*, **26**, 6777 (2012).
[44] F. Lin, D.E. Wang, Z.X. Jiang, Y. Ma, J. Li, R.G. Li, C. Li. *Energy Environ. Sci.*, **5**, 6400 (2012).
[45] C.Y. Wang, L.Y. Zhu, M.C. Wei, P. Chen, G.Q. Shan. *Water Res.*, **46**, 845 (2012).
[46] S. Leonard, P.M. Gannett, Y. Rojanasakul, D. Schwegler-Berry, V. Castranova, V. Vallyathan, X.L. Shi. *J. Inorg. Biochem.*, **70**, 239 (1998).
[47] K. Ranguelova, A.B. Rice, A. Khajo, M. Triquigneaux, S. Garantziotis, R.S. Magliozzo, R.P. Mason. *Free Radical Biol. Med.*, **52**, 1264 (2012).
[48] F. Lin, Y.N. Zhang, L. Wang, Y.L. Zhang, D.E. Wang, M. Yang, J.H. Yang, B.Y. Zhang, Z.X. Jiang, C. Li. *Appl. Catal., B*, **127**, 363 (2012).
[49] Y.B. Xie, L.M. Zhou, H.T. Huang. *Appl. Catal., B*, **76**, 15 (2007).
[50] F.Y. Ma, T. Shi, J. Gao, L. Chen, W. Guo, Y.H. Guo, S.T. Wang. *Colloids Surf., A*, **401**, 116 (2012).